

¹ **Full vector low-temperature magnetic measurements
of geologic materials**

Joshua M. Feinberg¹, Peter A. Solheid¹, Nicholas L. Swanson-Hysell^{1,2}, Mike

J. Jackson¹, and Julie A. Bowles^{1,3}

¹Institute for Rock Magnetism,

Department of Earth Sciences, University of
Minnesota, Minneapolis, Minnesota, USA

²Department of Earth and Planetary
Science, University of California, Berkeley,
California, USA

³Department of Geosciences, University of
Wisconsin, Milwaukee, WI, USA

3 Abstract. The magnetic properties of geologic materials offer insights
4 into an enormous range of important geophysical phenomena ranging from
5 inner core dynamics to paleoclimate. Often it is the low-temperature behav-
6 ior (<300 K) of magnetic minerals that provides the most useful and high-
7 est sensitivity information for a given problem. Conventional measurements
8 of low-temperature remanence are typically conducted on instruments that
9 are limited to measuring one **single axis** component of the magnetization vec-
10 tor and are optimized for measurements in strong fields. These instrumen-
11 tal limitations have prevented fully optimized applications and have moti-
12 vated the development of a low-temperature probe that can be used for low-
13 temperature remanence measurements **between 17 and 300K** along three **or-**
14 **thogonal** axes using a standard 2G Enterprises SQuID rock magnetometer.

15 In this contribution, we describe the design and implementation of this in-
16 strument and present data from five case studies that demonstrate the probe's
17 considerable potential for future research: a polycrystalline hematite sam-
18 ple, a polycrystalline hematite and magnetite mixture, a single crystal of mag-
19 netite, a single crystal of pyrrhotite and samples of Umkondo Large Igneous
20 Province diabase sills.

1. Introduction

21 Magnetic behavior at low temperatures (<300 K) is one of the most sensitive indicators
22 of the iron mineral phases and their concentrations and grain size distributions in nat-
23 ural samples. Changes in magnetocrystalline anisotropy and crystallographic structure
24 give rise to low-temperature transitions that are diagnostic of specific mineral phases.
25 The Morin transition of hematite (at ~262 K; *Morin* [1950]), the Verwey transition of
26 magnetite (at ~122 K; *Verwey* [1939]) and the Besnus transition of pyrrhotite (at ~32
27 K, *Besnus and Meyer* [1964]) are all diagnostic of common magnetic minerals that carry
28 remanence at Earth surface temperatures. Other phases that acquire remanence at low
29 temperature, such as siderite (with a Neél temperature of 38 K; *Frederichs et al.* [2003])
30 and superparamagnetic grains [*Worm and Jackson*, 1999], can also be readily identified
31 through their low-temperature behavior. In addition to the utility of low-temperature
32 data as a diagnostic tool for magnetic mineral identification and characterization, irre-
33 versible changes in remanence that are associated with cycling to low temperatures are
34 often used as a tool in paleomagnetic studies. Low-temperature steps in paleodirectional
35 and paleointensity study are applied in some protocols with the goal of preferentially
36 removing magnetic remanence held by multidomain grains and thereby isolating magne-
37 tizations held by single-domain grains [e.g., *Schmidt* [1993]; *Dunlop* [2003]; *Yamamoto*
38 *et al.* [2003]].

39 Low-temperature remanence experiments are routinely conducted on the Quantum De-
40 signs Magnetic Properties Measurement System (MPMS), most often with the intention
41 of revealing information about the dominant magnetic mineral phases and grain size dis-

tribution. While these instruments are adept at a range of low-temperature experiments, understanding the full behavior of a rock's natural remanence at low-temperature is hampered by the measurement capabilities being limited to a single axis and the instrument not providing an ultra-low field environment. If low-temperature measurements of a natural remanence (NRM) are desired using such instrumentation, great care must be taken to align the NRM with the measurement axis, and any directional change during thermal cycling will not be captured. In such an instrument, deviation from the single-axis will result in a measured magnetization that is less than the specimen's actual total magnetization.

In this contribution, we describe a low-temperature probe developed for use with superconducting rock magnetometers (SRM) at the Institute for Rock Magnetism (*IRM*), University of Minnesota. This instrument allows for three-axis **full-vector** measurements of magnetic remanence at temperatures between 300 and 17 K in low-field environments (<10 nT). It was developed with different engineering, but the same intent, as a low-temperature insert that has previously been implemented at the University of Rochester Paleomagnetic Laboratory [*Smirnov and Tarduno, 2011*].

2. Instrument design

In order to develop the capacity to make three-axis measurements of remanence in an ultra-low-field environment, a cryostat insert was developed at the *IRM* in cooperation with ColdEdge Technologies (Allentown, PA) (Figure 1). This low-temperature instrument (IRM-LTI) allows for three-axis measurements to be made between room temperature and \sim 17 K using horizontal-loading SRMs. There are many advantages to outfitting a superconducting rock magnetometer for measurements at low-temperatures. First, these instruments are specifically designed for three-axis remanence measurements, and ambient

64 fields are minimized using a superconducting lead shield. Nulling fields are applied by ex-
65 ternal coils while the shield cools to superconducting temperatures, ultimately trapping a
66 $\sim 2\text{-}3 \text{ nT}$ field along all three cardinal directions. Moreover modern SRM instruments uti-
67 lize DC-SQUID sensors that offer greater sensitivity than existing low-temperature mag-
68 netometers and susceptometers that rely on RF-SQUID sensors. A room-temperature,
69 open-ended bore is present in all 2G Enterprises magnetometers, allowing samples to be
70 easily moved into and out of the measurement region of the instrument.

71 The cryogenic insert is cooled by a pneumatically-driven SHI Displex SH-204 10K two-
72 stage cryocooler with a 73.7-cm copper cold tip extension and 3.8-cm diameter stainless
73 steel vacuum shroud (Figure 1). A 40.6-cm sapphire cold tip extension and sapphire
74 radiation shield are joined to the end of the copper extension in order to prevent any radio
75 frequency noise from traveling down the copper extension tip into the measurement region
76 of the magnetometer. Sapphire at low temperatures has a high thermal conductivity,
77 comparable to that of copper below 100K. A fiberglass vacuum shroud extension mounts
78 to the stainless steel shroud to provide a non-metallic extension to the vacuum insulation
79 space. Additional temperature control is provided by a non-inductively wound, 50-watt
80 cartridge heater integrated into the body of the probe and mounted out of the sensor
81 region, 40.6 cm away from the sample. The temperature inside the probe is monitored
82 directly at the sample using a non-magnetic, fiber-optic temperature sensor (NeoOptics
83 T1 probe) and two silicon diode sensors, one mounted on the copper cold tip extension
84 near the heater and one mounted on the first stage of the cryocooler to monitor the
85 radiation shield temperature. The probe assembly is mounted on a computer-controlled
86 translation table driven by a stepper motor for automated movement in and out of the

87 magnetometer, enabling background and sample measurements to be made throughout
88 cooling/warming cycles.

89 Samples can be affixed to the end of the sapphire extension tip in a variety of ways.
90 The goal is to maximize the thermal contact conductance between a sample and the
91 sapphire extension tip. In its simplest form, samples can be affixed using Kapton tape
92 ([a polyimide film with silicone bonding agent that maintains its adhesive properties even](#)
93 [at cryogenic temperatures](#)), but at temperatures below ~50 K, samples may lose efficient
94 thermal contact with the sapphire extension tip. Alternatively, a threaded copper sample
95 holder can be bonded to the end of the sapphire extension tip, allowing samples to be
96 held in thermal contact with the sapphire (Figure 1). Both of these methods allow for
97 samples with maximum cylindrical dimensions of 9 mm diameter and 5 mm height.

98 Measurements without any sample show maximum magnetizations of ca. 3×10^{-8}
99 Am² with some degree of temperature dependence (see supporting information). The
100 temperature-dependent magnetization of the [IRM-LTI](#) is largely repeatable, and empty
101 probe experiments are conducted prior to measurement runs to enable background sub-
102 traction if deemed necessary. Samples can be cooled from room temperature to ~17 K
103 over the course of about three hours and then [warmed](#) back to room temperature over
104 another three to four hours. Thus, the time required to collect low temperature data
105 using the IRM-LTI is roughly three times that required for the simplest low temperature
106 experiments on the MPMS. Alternatively, a user can define a more narrow temperature
107 range for more detailed studies of low temperature phenomena.

108 The approach and technical design of the LTI in this study (IRM-LTI) builds on ideas of
109 an earlier effort by the late William Goree of 2G Enterprises along with Aleksey Smirnov

and John Tarduno [*Smirnov and Tarduno, 2011*]. The key innovation of that collaborative effort was the design of a low-temperature instrument (that we will refer to as the ST-LTI) that could be inserted into a standard bore 2G Enterprises cryogenic rock magnetometer. In the ST-LTI, the sample was cooled by direct conduction in a bath of continually flowing liquid He. The sensors of the magnetometer were protected from the cooled low-temperature probe by a doubled-walled fiberglass tube, which was continually evacuated by a vacuum pump during measurements. Sample temperatures were monitored by a diode temperature sensor, which by necessity, was located about 10 cm behind the sample in order to avoid interference with the magnetometer pick-up coils.

The design of the LTI in this study (IRM-LTI) has several advantages and disadvantages when compared to the ST-LTI. One comparative disadvantage of the IRM-LTI is that the volume of instrumental material introduced into the measurement region of the magnetometer is greater than that of the ST-LTI, and background signals are consequently larger. The IRM-LTI is also intrinsically somewhat slower than the ST-LTI or the MPMS, since heat must be transported by solid-state conduction through a long rod rather than by advection in a fluid. Comparative advantages include: (1) because the IRM-LTI is moved via a translation table during measurements it is possible to quantify and adjust for background magnetization and magnetometer drift for each measurement; (2) this translation allows for the possibility of inline treatments, such as alternating-field demagnetization and acquisition of anhysteretic remanent magnetization and (3) utilizing a closed-cycle cryocooler systems allows the IRM-LTI to operate free of liquid helium. An additional positive aspect of the IRM-LTI is that it is currently available for

¹³² community use through the Institute for Rock Magnetism's Visiting Fellowship Program
¹³³ (<http://www.irm.umn.edu/IRM/applying.html>).

3. Case studies using the instrument

¹³⁴ The five case studies that follow serve three primary purposes:
¹³⁵ 1. To demonstrate that the temperature-dependent intensity data acquired using the
¹³⁶ IRM-LTI is virtually identical to that acquired using MPMS instruments (as shown by
¹³⁷ *Smirnov and Tarduno* [2011] for the ST-LTI), which should give confidence to potential
¹³⁸ users.

¹³⁹ 2. To demonstrate the utility of three-axis full-vector magnetic measurements in several
¹⁴⁰ different rock magnetic and paleomagnetic applications. In the course of doing so, novel
¹⁴¹ results have been obtained.

¹⁴² 3. To inspire new uses for the IRM-LTI, and in some instances we have provided sug-
¹⁴³ gestions for future studies that we have not yet explored.

3.1. Polycrystalline Hematite

¹⁴⁴ A [metamorphic schist containing](#) polycrystalline hematite from Labrador, Canada with
¹⁴⁵ a strong foliation was pulsed in a 1.2 T field approximately perpendicular to the folia-
¹⁴⁶ tion plane to impart an isothermal remanent magnetization (IRM) ([using an ASC Model](#)
¹⁴⁷ [IM-10-30 Impulse Magnetizer](#)). The strong shape-preferred alignment of the hematite
¹⁴⁸ grains in this polycrystalline sample allows us to explore whether its remanence direc-
¹⁴⁹ tion shifts after cooling through the Morin transition. Room temperature remanence in a
¹⁵⁰ single crystal of hematite falls within the basal plane, while remanence below the Morin
¹⁵¹ transition is oriented along the normal to this plane. After being imparted, the IRM was

152 cycled from room-temperature to \sim 130 K using the IRM-LTI in conjunction with an SRM
153 (Figure 2A). The specimen underwent a significant loss of remanence as it cooled through
154 the Morin transition which is partially recovered as the sample warmed back through the
155 transition temperature (Figure 2A,C). During this low-temperature cycling, the sample's
156 directional remanence remained subparallel to the foliation normal (i.e. on average ap-
157 proximately parallel to the c axes of the individual crystals) and did not migrate towards
158 the plane of the magnetic fabric (Figure 2B). Even without any background correction,
159 the majority of the remanence lies close to the z-axis of the stereonet. However, there is a
160 15-degree deflection in inclination away from 90 degrees (Figure 2B). This deflection can
161 be attributed to the magnetization of the IRM-LTI itself. The IRM-LTI's magnetization
162 and low-temperature behavior can be important when measuring **weak** remanence sam-
163 ples and background subtraction is necessary. This particular experiment was conducted
164 when the IRM-LTI was outfitted with a relatively magnetic silicon diode thermometer
165 that contributed to a background signal of \sim 10⁻⁶ Am². Subsequent improvements to the
166 instrumental set-up have led to the current use of a far less magnetic fiber-optic temper-
167 ature sensor that contributes \sim 10⁻⁸ Am² to the background signal. By measuring the
168 low-temperature cycling of the IRM-LTI without a mounted sample, we can characterize
169 the background of the instrument and then subtract this influence from the measured
170 sample data. When this background subtraction is done for the hematite sample, the
171 data are tightly grouped near 90 degrees of inclination, illustrating the uniformity of the
172 magnetization in the direction of the applied IRM before and after cooling through the
173 Morin transition (Figure 2B). The fact that the **remanence** remains parallel to the original
174 applied field direction throughout the experiment suggests either that the alignment of the

¹⁷⁵ hematite crystals was not perfect (otherwise the remanence would have fallen within the
¹⁷⁶ basal plane) and/or that the remanence was held by defects within hematite.

¹⁷⁷ In this instance, the data collected with the three-axis IRM-LTI are very similar to those
¹⁷⁸ collected with a 1-axis MPMS [as part of a standard low-temperature cycling of room-](#)
¹⁷⁹ [temperature saturation IRM](#)(Figure 2C). The ratio of the room temperature remanence
¹⁸⁰ before and after low temperature cycling is nearly identical. One subtle difference between
¹⁸¹ the two data sets is the slightly lower estimates of the Morin transition temperature on
¹⁸² cooling and warming from the IRM-LTI (257.4 K) as compared to the MPMS (259.4 K;
¹⁸³ see supporting online materials for details on these estimates of transition temperature).
¹⁸⁴ One possible explanation for this minor difference is a small thermal lag within the IRM-
¹⁸⁵ LTI. Additional measurements at a variety of cooling rates will test this explanation in
¹⁸⁶ the future.

3.2. Mixed assemblage of hematite and magnetite

¹⁸⁷ A polycrystalline hematite specimen containing trace amounts of magnetite was im-
¹⁸⁸ parted with a 1.2 T IRM. Following this treatment, the specimen was cooled to ~20
¹⁸⁹ K and then warmed back to room temperature inside the probe (Figure 3). This mea-
¹⁹⁰ surement is roughly equivalent to the room-temperature saturation isothermal remanent
¹⁹¹ magnetization (RT-SIRM) experiments routinely conducted on MPMS instruments, and
¹⁹² allows one to explore how the remanence of each phase evolves during low temperature
¹⁹³ cycling from room temperature to 20 K. The effects of the Morin and Verwey transitions
¹⁹⁴ are quite prominent as the sample was cycled to and from low-temperature while the
¹⁹⁵ direction of the magnetization did not vary (Fig. 3A).

196 After completion of the IRM-LTI experiment, a 1.2-T IRM was again applied to the
197 specimen and then thermally cycled using an MPMS. Comparison of the IRM-LTI and
198 MPMS data shows the results to be quite similar (Fig. 3B). Two subtle differences can
199 be seen between the two data sets: (1) there is a systematic ~ 2 K shift of the Morin and
200 Verwey transitions towards cooler temperatures in the IRM-LTI data compared to the
201 MPMS data (see supporting online materials for details), as was seen with the Labrador
202 hematite sample (Figure 2C), and similar to the temperature offset observed by Smirnov
203 and Tarduno in the ST-LTI experiments; (2) the magnitude of the magnetization is slightly
204 less for the MPMS data than the total vector of the three-axis IRM-LTI data, suggesting
205 that some of the magnetization may have been off-axis during the MPMS experiment and
206 thereby not detected by the single-axis measurement capabilities of that instrument.

207 In future studies, the IRM-LTI can be used to disentangle the remanence held by each
208 of these phases by imparting specimens with multiple, mutually perpendicular magnetiza-
209 tions, similar in style to a Lowrie test [Lowrie, 1990], where the remanence associated with
210 specific phases is forced to lie along different cardinal directions. In this way, the IRM-
211 LTI may provide a unique method for non-destructive exploration of the tempera-
212 dependent magnetic behavior of mixed magnetic mineral assemblages.

3.3. Single crystal of magnetite

213 A square-based pyramid was cut from a magnetite octahedron to explore the directional
214 behavior of remanence for a single crystal of multidomain magnetite during low tempera-
215 ture cycling using the IRM-LTI. The 2-mm subspecimen used in this study was prepared
216 using a low-speed saw to remove the pyramid from the top of a natural magnetite octa-
217 hedron that originated in the Central African Republic (mined and sold by [Ikon Mining](#)

218 Co.). Three experiments (or 'Series') were conducted, each of which consisted of applying
219 a strong (1.2 T) IRM in a distinct direction and then cycling that magnetization to low-
220 temperature (20 K) and back. A schematic drawing of the specimen and its orientation
221 relative to the measurement axes of the superconducting rock magnetometer (SRM) and
222 to the orientations of three separate 1.2 T IRMs is shown in Figure 4A. The low temper-
223 ature cycling of the isothermal remanence applied to the specimen is described in detail
224 below, but it is important to note that there are multiple sources of orientation error
225 that are inherent to the measurements. First, despite the care taken during specimen
226 preparation, it is likely that the square base of the pyramid was not cut exactly parallel
227 to the (100) of magnetite and may be misaligned by < 10°. Such an error will affect all of
228 the directional IRM experiments. Second, for each IRM there may be a small < 10° error
229 between the orientation of the applied field and its targeted crystallographic direction.
230 Third, there is also a small (< 5°) error associated with placement of the specimen back
231 on the end of the IRM-LTI after each successive IRM. This latter error should only be
232 rotational around the Z-axis of the magnetometer.

233 We attempted to impart the IRMs along the [-111], [100], and [0-1-1] of magnetite be-
234 cause these directions correspond to magnetocrystalline easy, hard, and intermediate axes,
235 respectively, at room temperature. As magnetite cools below the Verwey transition (T_V),
236 the mineral experiences a first-order phase transition where its crystal symmetry changes
237 from cubic (c) to monoclinic (m). The orientations of the a , b , and c axes of the resulting
238 monoclinic magnetite will depend on the magnetic environment in which this transition
239 occurs, but by convention are described as $[001]_m//[001]_c$, $[100]_m//[110]_c$, and $[010]_m//[-$

²⁴⁰ 110]_c (e.g., *Kasama et al.* [2010]). The easy, intermediate, and hard magnetocrystalline
²⁴¹ axes for monoclinic magnetite are [001]_m, [010]_m, and [100]_m, respectively.

²⁴² Figure 4B shows the directional results of the low temperature cycling of the three sep-
²⁴³ arate IRM experiments, while Figure 4C shows the magnitude of total magnetization as
²⁴⁴ a function of temperature (as opposed to the X, Y, and Z components). The alignment
²⁴⁵ of the IRM remanence with the intended magnetocrystalline axes of the magnetite is
²⁴⁶ broadly similar to the experimental scheme. There are no dramatic changes in remanence
²⁴⁷ direction during low temperature cycling regardless of the orientation of the applied IRM.
²⁴⁸ During cooling from room temperature the remanence of all three IRMs decreases towards
²⁴⁹ the isotropic point ($T_K = 130$ K) and Verwey transition ($T_V = 110$ to 120 K), reaching
²⁵⁰ a minimum at ~ 118 K (Figure 4C). The extent of this remanence drop is slightly direc-
²⁵¹ tionally dependent: the percent loss in remanence from 260 K to the Verwey transition
²⁵² minima for the IRMs imparted along [-111], [100], and [0-1-1] are 68%, 75%, and 72%,
²⁵³ respectively. Thus, the remanence imparted along the cubic magnetocrystalline easy axis
²⁵⁴ was marginally more resistant to low temperature demagnetization than those imparted
²⁵⁵ along the intermediate or hard axes. On continued cooling through T_V , the remanence
²⁵⁶ increases abruptly and significantly (Figure 4C), unlike the behavior commonly observed
²⁵⁷ for polycrystalline MD powder samples in MPMS experiments, but similar to that found
²⁵⁸ in previous single-crystal measurements [e.g., *Özdemir and Dunlop* [1999]; *Smirnov and*
²⁵⁹ *Tarduno* [2011]]. The magnitude of remanence below the Verwey transition is also some-
²⁶⁰ what anisotropic with the ratio of remanence at 20 K to that at 260 K for each IRM
²⁶¹ at 53%, 61%, and 56%, respectively. Thus, remanence was more readily inherited by
²⁶² monoclinic magnetite when the original room-temperature IRM is applied parallel to its

263 monoclinic magnetocrystalline easy axis direction ($[001]_m$ or $[001]_c$). A third metric of
264 anisotropy is seen after cycling back to 260 K, where the recovered remanence for the
265 IRMs imparted along [-111], [100], and [0-1-1] is 44%, 48%, and 40%, respectively. In this
266 context, the most efficient remanence recovery occurred when the original IRM was im-
267 parted along the cubic magnetocrystalline hard axis. This persistent remanence is likely
268 pinned by crystalline imperfections in the magnetite, such as dislocation networks (as
269 recently imaged by *Lindquist et al.* [in review]). The absolute value of the remanence on
270 warming back to room temperature is nearly identical for all three IRM treatments (Figure
271 4C), suggesting that regardless of the orientation of the initial IRM, after passing twice
272 through T_V and T_K the final arrangement of domain walls in the specimen has achieved a
273 common low-energy configuration. These results also show the incomplete nature of low-
274 temperature demagnetization associated with MD-sized grains. However, as is shown in
275 ARM data applied to an assemblage of MD magnetite in a coarse-grained diabase sample
276 below, it is likely that the portion of magnetization that was demagnetized is the lowest
277 coercivity fraction. In this case study, we examine a single, large MD grain and show
278 that a minimum of a third of its remanence is routinely retained after low-temperature
279 cycling. The low-temperature behavior of MD magnetite is further discussed below in
280 section 3.5, and has important implications for paleomagnetic and paleointensity studies
281 that use low-temperature demagnetization steps to minimize the unwanted contributions
282 from MD grains.

283 The data acquired by the IRM-LTI also allow users to see subtle, but important details
284 that are often lost in one-axis MPMS measurements. For example, the sudden drop in
285 remanence as the magnetite passes through its Verwey transition near 118 K, as well as

the more progressive remanence loss as magnetite passes through its isotropic point near 130 K are both well-resolved in the three-axis data (Fig. 5). Another interesting observation from the three-axis data is the change in the remanence direction in series 2 (where the 1.2 T IRM was applied approximately parallel to the [100] direction) wherein there is subtle clockwise movement on cooling that is reversible on warming. There are two distinct clusters of directions: one cluster is defined by all data collected above 115 K, while the second cluster is comprised of all data collected below 115 K. Measurements collected at 115 K on both cooling and warming are at an intermediate position (Figure 5). The vector component diagram in Figure 5C also shows this behavior along with the concomitant change in intensity before and after the Verwey transition. The crystallographic origins of this directional movement require further study, but one likely influence is the reorganization of ferroelastic twins as the sample is converted from one crystal system to the other [e.g., *Kasama et al.* [2010]].

3.4. Single crystal of pyrrhotite

A single crystal of pyrrhotite measuring ~2.5 by ~3.5 by ~4.5 mm was used to explore the directional behavior of remanence for multidomain pyrrhotite during low-temperature cycling using the IRM-LTI (Figure 6A). Pyrrhotite often occurs in nature as intergrowths of hexagonal and monoclinic iron sulfide, the latter of which is ferrimagnetic at room temperature. Monoclinic pyrrhotite experiences a dramatic change in its magnetic properties at ~35 K (*Besnus and Meyer* [1964], Figure 6B); the underlying crystallographic and/or magnetocrystalline changes are still debated [*Wolfers et al.*, 2011; *Kind et al.*, 2013]. The details of the mineral's crystal symmetry and internal microstructures are highly complex owing to nonstoichiometry in the Fe_{1-x}S system and non-regular ordering (or 'incommen-

surate' ordering) of vacancies within the crystal lattice. Crystallographers frequently take a simplified view of the mineral in referring to its crystal symmetry as 'pseudohexagonal.' Above the Besnus transition, pyrrhotite exhibits a 'hard' magnetic axis along the c direction and remanence tends to lie within the basal plane defined by the a_1 , a_2 , and a_3 axes (*Martín-Hernández et al. [2008]*). A secondary electron micrograph of the single-crystal specimen used in this study is shown in Figure 6A (collected with a JEOL 6500 FEG-SEM operated at 20 kV with a working distance of 22.8 mm). The orientations of the crystal's pseudohexagonal crystallographic axes were measured using electron backscatter diffraction (EBSD) and are shown in Figure 6A. No evidence of monoclinic-hexagonal intergrowths were observed during EBSD analyses, which provides further evidence for the single crystal nature of this sample. Prior to measurement in the IRM-LTI, the sample was oriented such that the a_1 axis was subparallel to the X-axis of the magnetometer. The remanence of the sample was noted and then the threaded copper sample holder was tightened onto the sample mounting surface to ensure thermal contact, resulting in a counter-clockwise rotation of the a_1 axis of 10° to 30°. IRMs were imparted to the sample in a number of orientations prior to low temperature cycling in the IRM-LTI, and the intended directions are shown as blue points in the equal area plots in Figure 6C. As was the case with the single-crystal magnetite measurements, there are likely small angular errors between the actual and intended applied field directions for IRM acquisition.

Figure 6C shows the directions throughout low-temperature demagnetization of three separate 1.2-T IRMs imparted along different crystallographic directions. The leftmost equal area plot in Figure 6C shows the low-temperature demagnetization of an IRM imparted along an angle bisecting the pyrrhotite a_1 and c axes. The resulting remanence

falls almost directly along the a_1 axis Figure 6C. This difference in applied field direction and the acquired remanence is likely due to the strong anisotropy given that remanence in pyrrhotite prefers to lie within the basal plane of the pseudohexagonal structure. During cooling and warming the remanence direction remains largely unchanged, but does track slightly along a great circle that includes the c -axis. After passing through the Besnus transition on cooling the remanence at 20 K is only 10% of the value at 290 K. After warming back to 290 K, the final residual remanence is 18% of the original remanence at 290 K (see supporting online materials).

The middle equal area plot in Figure 6C shows an IRM imparted along the c -axis. The resulting remanence falls along the $-a_1$ direction, again indicating the strong tendency at room temperature for remanence in pyrrhotite to lie within the basal plane. As in the case for the low-temperature cycling the IRM that bisected c and a_1 , the remanence direction remained relatively stable during low temperature cycling. However, after passing through the Besnus transition on cooling the remanence of this IRM at 20 K is 25% of the value at 290 K. After warming back to 290 K, the final residual remanence is 17% of the original remanence at 290 K (Figure 6B). Thus, an IRM applied along the pyrrhotite c -axis allows for a greater percentage of its remanence to be retained after cooling through the Besnus transition.

The rightmost equal area plot in Figure 6C shows an IRM imparted along an angle that bisects the a_1 and $-a_3$ directions. In this instance the resulting remanence direction appears to be oriented roughly parallel to the applied field direction, suggesting that pyrrhotite remanence is not constrained to lie solely along the a_i axes, but may be oriented supaparallel to the applied field within the basal plane. After passing through the Besnus transition

354 on cooling the remanence at 20 K is 18% of the value at 290 K. After warming back to
355 290 K, the final residual remanence is 22% of the original remanence at 290 K. Thus, a
356 higher percentage of remanence seems to be retained after cycling through the Besnus
357 transition if an IRM is applied along a direction within the basal plane.

358 It is worth noting that no evidence of a self-reversal was observed in our IRM experi-
359 ments on pyrrhotite. This phenomenon has been observed to occur in large single crystals
360 of pyrrhotite that are either internally twinned (e.g., [Zapletal, 1992]) or partially oxi-
361 dized (e.g., [Bina and Daly, 1994]), whereas the crystal the pyrrhotite single crystal in
362 this study is untwinned and unoxidized.

3.5. Samples from the interior of Umkondo large igneous province sills

363 Many rocks carry complex multicomponent natural remanent magnetizations, with dif-
364 ferent generations of magnetization acquired at different times by separate mechanisms
365 and carried in varying proportions by different populations of magnetic grains. For such
366 heterogeneous magnetizations, significant directional changes may accompany passage
367 through transitions and isotropic points as different components are affected according
368 to the mineralogy, defect structures, and grain sizes of their carriers. Just as continuous
369 high-temperature thermal demagnetization can provide crucial observations for correctly
370 interpreting a sample's remanence [Wack and Matzka, 2007; Coe et al., 2014], full-vector
371 measurements during low-temperature cycling of such samples may also provide a new
372 means of disentangling a rock's complex magnetization history.

373 Bulk rock samples containing large populations of randomly-oriented magnetic crys-
374 tals carrying a univectorial remanence (i.e., a magnetization acquired through a single
375 process, in a relatively constant field orientation), are not expected to show large di-

376 rectional changes while passing through magnetic transitions. In such a scenario, the
377 directional changes associated with the individual crystals should average out, and only
378 a change in the magnitude of the remanence should be observed. This is the case for
379 specimen PW15-4d, a coarse-grained diabase sill from the ~1.1 Ga Umkondo Province
380 of Botswana [Hanson *et al.*, 2004]. Room-temperature alternating-field demagnetization
381 experiments show that the NRM decays in a univectorial manner (Figure 7A). Traditional
382 low-temperature demagnetization experiments involving submersion in a liquid N₂ bath
383 result in a 52% loss in NRM intensity (Figure 7A), suggesting that a significant fraction
384 of the remanence is held by multidomain grains. Low-temperature cycling of the NRM in
385 the IRM-LTI on a sister specimen from the same core shows that the remanence direction
386 remains stationary while the intensity decreases significantly such that it is only 21% of
387 the initial NRM after cooling through the Verwey transition. The magnetization recov-
388 ers to 52% of the original NRM value upon warming back to room temperature (Figure
389 7B) resulting in a similar overall remanence loss as the liquid nitrogen bath on the sister
390 specimen.

391 In order to explore whether low-coercivity magnetite loses its remanence at similar
392 temperatures to higher-coercivity magnetite, this same specimen was given two mutually
393 perpendicular anhysteretic remanent magnetizations (ARMs; Figure 8). First, the spec-
394 imen was given an ARM along its negative Z-axis (200 mT AF with a 100 μ T DC bias
395 field). Then the specimen was imparted with a second more weakly held ARM along
396 its negative x-axis (5 mT AF with a 200 μ T DC bias field). This second ARM targeted
397 only those grains in the sample with coercivities \leq 5 mT, and hence is a partial ARM
398 (pARM). In contrast, the first ARM applied along the z-axis is held by higher coercivity

399 grains ranging between 5 and 200 mT (referred to as ' ARM_Z ' henceforth). On thermal
400 cycling in the IRM-LTI, the remanence associated with ARM_Z behaves in a manner sim-
401 ilar to what is commonly observed in single-axis MPMS measurements, where remanence
402 begins to decrease at ~ 225 K and then decreases at an accelerating rate as it approaches
403 T_V (Figure 8A). This pattern of remanence loss parallels the changes in the dominant
404 magnetocrystalline energy term for cubic magnetite (K_1) (Figure 8C). The isotropic point
405 for magnetite, T_K , occurs near 130 K when K_1 changes from negative to positive. Thus,
406 this pattern of remanence loss in magnetite during cooling is actually a two-stage process
407 involving passage through both T_K and T_V . During warming, the remanence associated
408 with the ARM_Z recovers to 71% of its original value. This low-temperature memory is
409 significant and is typical for single-domain and pseudo-single-domain grains, which are
410 able to preserve their original remanence owing to shape anisotropy and pinned domain
411 walls [Dunlop and Özdemir, 1997]. It is also likely that some of this remanence is held by
412 multidomain grains with regions of high defect density that produce pinning coercivities
413 higher than 5 mT.

414 By contrast, the pattern of remanence loss associated with the lower coercivity p ARM
415 is significantly different from that of the ARM_Z (Figure 8A,B). The lower coercivity re-
416 manence experiences a linear decrease from room temperature to T_V that is seemingly
417 unaffected by the rate of change in the K_1 magnetocrystalline energy term (Figure 8C).
418 This style of low temperature demagnetization behavior is novel and to our knowledge
419 has not been observed in earlier studies of magnetite-bearing rocks, although Muxwor-
420 thy et al. [2003] did observe systematic changes in the shapes of $M(T)$ cooling curves
421 for pARMs acquired over different coercivity windows, in magnetites of differing grain

422 sizes. Importantly, this behavior would be undetected in a conventional MPMS RT-SIRM
423 measurement. There is no recovery of this remanence during warming back to room tem-
424 perature (Figure 8A,B), suggesting that this remanence was held by multidomain grains
425 whose domain wall configurations were dramatically rearranged during cycling through
426 both T_K and T_V . The final remanence direction following low-temperature cycling of the
427 $\text{ARM}_Z + \text{pARM}_X$ is very similar to the ARM_Z direction prior to imparting pARM_X . This
428 result demonstrates the effectiveness of low-temperature demagnetization for the removal
429 of remanence held by low-coercivity grains.

430 Some of the specimens from the Umkondo province sills show significant directional
431 changes after thermal cycling in liquid N₂. Figure 9 shows one such specimen, PW10-7a,
432 whose NRM direction shifted by 64° after the low-temperature demagnetization (LTD)
433 step. A conventional MPMS RT-SIRM measurement (see supporting online materials),
434 shows that 67% of the room temperature remanence is lost through low-temperature
435 demagnetization. However, the IRM-LTI provides a more complete picture, capturing this
436 same broad behavior, but also documenting the progressive directional change throughout
437 the experiment (Fig. 9). After passing through T_V , the remanence direction remains
438 relatively constant during cooling to 20 K and subsequent rewarming to T_V . However,
439 during warming from T_V to room temperature the specimen's remanence direction shifts
440 dramatically towards expected Umkondo orientations as the low temperature memory
441 held by SD and PSD grains is preferentially recovered over magnetization held by MD
442 grains that is not recovered. As a result, the overprint, secondary to the primary thermal
443 remanent magnetization is largely, although not entirely, removed. These three-axis data
444 demonstrate the effectiveness of low-temperature cycling as a tool for demagnetization of

445 remanence held by MD grains. Furthermore, these data give a glimpse into the "black box"
446 of progressive remanence change that occurs during routine liquid N₂ demagnetization of
447 paleomagnetic samples.

4. Future directions

448 This study presents several examples demonstrating the utility of low-temperature re-
449 manence cycling using the IRM-LTI, but there are a multitude of additional research
450 directions that can be explored using this instrument. From an experimental perspective,
451 one of the more exciting applications for the IRM-LTI is the potential for in-line treatments
452 at low temperatures. Examples include alternating field demagnetization and acquisition
453 of anhysteretic remanence magnetization (ARM) or IRM. Such treatments would allow
454 researchers to explore changes in the coercivity distributions of samples above and below
455 important mineral transitions, such as the Morin, Verwey, and Besnus transitions. For
456 nanoparticle populations, the joint distribution of grain size and microcoercivity $f(V, H_{k0})$
457 can be obtained by AF demagnetization of weak-field TRMs at a set of low temperatures
458 [c.f., *Dunlop and West [1969]*]. To enable such new experimental capabilities, the con-
459 struction of in-line coils is currently underway at the *IRM*. Additionally, as alluded to
460 in Section 3.2, the IRM-LTI also has the potential to run three-axis Lowrie style ther-
461 mal cycling experiments that can enable users to unmix the low-temperature remanence
462 held by populations of different phases and grain sizes with greater confidence than pos-
463 sible with a single-axis instruments. This approach will provide information analogous to
464 that obtained in traditional Lowrie tests, but without the potential for mineral alteration
465 typically associated with thermal demagnetization experiments above room temperature.

466 The experimental flexibility of the IRM-LTI may make it possible to address many of
467 the questions regarding fundamental magnetic behavior in important minerals such as
468 magnetite, maghemite, titanomagnetite, hematite, [greigite](#), and pyrrhotite. The IRM-
469 LTI allows researchers to observe full-vector remanence changes as minerals pass through
470 isotropic points, ordering temperatures, and blocking and unblocking temperatures. Pro-
471 cesses such as TRM acquisition can be explored by measuring the remanence acquired
472 by populations of superparamagnetic grains. Similarly, the effects of cooling rate on the
473 intensity of remanence can be directly observed by modifying the rate at which specimens
474 are cooled. By preparing specimens with varying degrees of mineral alignment it may also
475 be possible to quantify the anisotropy of remanence. This is by no means an exhaustive
476 exposition of the possible rock magnetic applications, but we hope that it illustrates the
477 research potential of the instrument.

478 The IRM-LTI can also provide complementary information to planetary scientists trying
479 to isolate the primary magnetization of meteorites in order to learn more about the condi-
480 tions that existed during the early history of the solar system. The assemblage of magnetic
481 minerals found within meteorite samples is frequently far more complex than that found
482 in terrestrial samples. Alloys of Fe, Ni, and S are common, as are varying concentra-
483 tions of magnetite and titanomagnetite. The effects of shock on remanent magnetization
484 further compound the difficulties of interpreting a meteorites complex thermomagnetic
485 history. One process that has not received as much attention is the effect of low temper-
486 ature thermal cycling on the remanent magnetism of the constituent magnetic minerals.
487 The orbits of most asteroids and comets are eccentric, which guarantees that these ob-
488 jects will experience heating and cooling cycles during the course of their orbit around

489 the Sun. Another process that may affect the magnetization of meteorites is inverse ther-
490 moremanent magnetization, which is acquired as magnetite is warmed through the Verwey
491 transition or isotropic point [Dunlop, 2006]. This type of remanence could be acquired
492 in Earth's field as meteorites warm to Earth surface temperatures and could contaminate
493 paleointensity measurements. The IRM-LTI's low-temperature, three-component system
494 allows researchers to design experiments to observe remanence changes that could result
495 from thermal perturbations experienced by meteorites as they pass by the Sun (at solar
496 perigee) or as they enter Earth's atmosphere.

497 These applications form the basis for decades of potential future research; much more
498 than could ever be accomplished by the authors of this study. The instrument was designed
499 with a philosophy of making it affordable to other research groups and to be broadly
500 compatible with horizontal-loading 2G Enterprises cryogenic magnetometers that are used
501 in the majority of paleomagnetic laboratories. The IRM-LTI is currently housed at the
502 Institute for Rock Magnetism at the University of Minnesota, where it is available to
503 the international scientific community through the lab's NSF Visiting Fellowship program
504 (<http://www.irm.umn.edu/IRM/categories.html>). It is hoped that this study will inspire
505 colleagues to visit the IRM in order to **use** the instrument to advance their own research
506 programs.

507 **Acknowledgments.**

508 Bill Goree's career of developing and commercializing superconducting rock magne-
509 toometers for paleo- and rock magnetism continues to leave a substantial impact on our
510 discipline. This project builds on his vision of a low-temperature insert that just before
511 his passing in 2007 he envisioned would be best implemented with a liquid-free cyro-

512 cooler system. John Tarduno encouraged the development of this type of insert and
513 provided valuable input based on his lab's experience with their flow-through system.
514 Richard Hanson played an important role in the field expedition during which samples
515 were collected from Umkondo Sills. Functions from the open source PmagPy project
516 (<https://github.com/ltauxe/PmagPy>) were used extensively for data plotting and we are
517 grateful to the project's lead developer Lisa Tauxe. **The manuscript benefitted from re-**
518 **views by Mark Dekkers, Aleksey Smirnov and one anonymous researcher.** This research
519 was funded by EAR-0929807 to J.M.F., EAR-1045635 to N.L.S.-H., and by support of
520 the IRM by the NSF/EAR Instruments and Facilities program. This is IRM contribution
521 1409.

References

- 522 Besnus, M. J., and A. J. Meyer (1964), Nouvelles données expérimentales sur le
523 magnétisme de la pyrrhotine naturelle, in *Proc. Int. Conf. Mag.*, vol. 20, pp. 507–511.
- 524 Bickford, L. R., J. M. Brownlow, and R. F. Penoyer (1957), Magnetocrystalline anisotropy
525 in cobalt-substituted magnetite single crystals, *Proceedings of the IEE - Part B: Radio*
526 *and Electronic Engineering*, 104(5), 238–244, doi:10.1049/pi-b-1.1957.0038.
- 527 Bina, M., and L. Daly (1994), Mineralogical change and self-reversed magnetizations in
528 pyrrhotite resulting from partial oxidation; geophysical implications, *Physics of the*
529 *Earth and Planetary Interiors*, 85(1–2), 83–99, doi:[http://dx.doi.org/10.1016/0031-9201\(94\)90009-4](http://dx.doi.org/10.1016/0031-9201(94)90009-4).
- 531 Coe, R. S., N. A. Jarboe, M. Le Goff, and N. Petersen (2014), Demise of the rapid-
532 field-change hypothesis at Steens Mountain: The crucial role of continuous ther-
533 mal demagnetization, *Earth and Planetary Science Letters*, 400(0), 302–312, doi:

534 10.1016/j.epsl.2014.05.036.

535 Dunlop, D., and Ö. Özdemir (1997), *Rock Magnetism: Fundamentals and frontiers*, Cam-
536 bridge University Press, Cambridge, UK.

537 Dunlop, D. J. (2003), Stepwise and continuous low-temperature demagnetization, *Geo-*
538 *phys. Res. Lett.*, 30(11).

539 Dunlop, D. J. (2006), Inverse thermoremanent magnetization, *Journal of Geophysical*
540 *Research: Solid Earth*, 111(B12), B12S02, doi:10.1029/2006JB004572.

541 Dunlop, D. J., and G. F. West (1969), An experimental evaluation of single domain the-
542 *ories, Reviews of Geophysics and Space Physics*, 7, 709, doi:10.1029/RG007i004p00709.

543 Frederichs, T., T. von Dobeneck, U. Bleil, and M. J. Dekkers (2003), Towards the identi-
544 fication of siderite, rhodochrosite, and vivianite in sediments by their low-temperature
545 magnetic properties, *Physics and Chemistry of the Earth, Parts A/B/C*, 28(16–19),
546 669–679, doi:10.1016/S1474-7065(03)00121-9.

547 Hanson, R., J. Crowley, S. Bowring, J. Ramezani, W. Gose, I. Dalziel, J. Pancake, E. Sei-
548 del, T. Blenkinsop, and J. Mukwakwami (2004), Coeval large-scale magmatism in the
549 Kalahari and Laurentian Cratons during Rodinia assembly, *Science*, 304, 1126–1129,
550 doi:10.1126/science.1096329.

551 Kasama, T., N. S. Church, J. M. Feinberg, R. E. Dunin-Borkowski, and R. J. Harrison
552 (2010), Direct observation of ferrimagnetic/ferroelastic domain interactions in magnetite
553 below the Verwey transition, *Earth and Planetary Science Letters*, 297(1-2), 10–17, doi:
554 10.1016/j.epsl.2010.05.004.

555 Kind, J., I. García-Rubio, M. Charilaou, N. R. Nowaczyk, J. F. Löffler, and A. U. Gehring
556 (2013), Domain-wall dynamics in 4C pyrrhotite at low temperature, *Geophysical Journal*

- 557 International, 195(1), 192–199, doi:10.1093/gji/ggt262.
- 558 Lindquist, A., J. Feinberg, R. Harrison, J. Loudon, and A. Newell (in review), Domain wall
559 pinning and dislocations: Investigating magnetite deformed under conditions analogous
560 to nature using transmission electron microscopy, *Journal of Geophysical Research, Solid*
561 *Earth*.
- 562 Lowrie, W. (1990), Identification of ferromagnetic minerals in a rock by coercivity and
563 unblocking temperature properties, *Geophys. Res. Lett.*, 17(2), 159–162.
- 564 Martín-Hernández, F., M. J. Dekkers, I. M. A. Bominaar-Silkens, and J. C. Maan
565 (2008), Magnetic anisotropy behaviour of pyrrhotite as determined by low- and high-
566 field experiments, *Geophysical Journal International*, 174(1), 42–54, doi:10.1111/j.1365-
567 246X.2008.03793.x.
- 568 Morin, F. J. (1950), Magnetic susceptibility of α -Fe₂O₃ and α -Fe₂O₃ with added titanium,
569 *Physical Review*, 78, 819–820.
- 570 Muxwworthy, A. R., and E. McClelland (2000), Review of the low-temperature magnetic
571 properties of magnetite from a rock magnetic perspective, *Geophysical Journal International*,
572 140, 101–114.
- 573 Muxwworthy, A. R., D. J. Dunlop, and Ö. Özdemir (2003), Low-temperature cycling of
574 isothermal and anhysteretic remanence: microcoercivity and magnetic memory, *Earth*
575 and *Planetary Science Letters*, 205(3–4), 173–184, doi:10.1016/S0012-821X(02)01039-7.
- 576 Özdemir, Ö., and D. J. Dunlop (1999), Low-temperature properties of a single crystal of
577 magnetite oriented along principal magnetic axes, *Earth and Planetary Science Letters*,
578 165(2), 229–239, doi:10.1016/S0012-821X(98)00269-6.

- 579 Schmidt, P. W. (1993), Palaeomagnetic cleaning strategies, *Physics of the Earth and*
580 *Planetary Interiors*, 76(1–2), 169–178, doi:10.1016/0031-9201(93)90066-I.
- 581 Smirnov, A. V., and J. A. Tarduno (2011), Development of a low-temperature insert for
582 the measurement of remanent magnetization direction using superconducting quantum
583 interference device rock magnetometers, *Geochem. Geophys. Geosyst.*, 12(4).
- 584 Verwey, E. J. W. (1939), Electronic conduction of magnetite (Fe_3O_4) and its transition
585 point at low temperatures, *Nature*, 144, 327–328.
- 586 Wack, M., and J. Matzka (2007), A new type of a three-component spinner magnetometer
587 to measure the remanence of rocks at elevated temperature, *Earth, Planets, and Space*,
588 59, 853–862.
- 589 Wolfers, P., G. Fillion, B. Ouladdiaf, R. Ballou, and P. Rochette (2011), The
590 pyrrhotite 32K magnetic transition, *Solid State Phenomena*, 170, 174–179, doi:
591 10.4028/www.scientific.net/SSP.170.174.
- 592 Worm, H.-U., and M. Jackson (1999), The superparamagnetism of Yucca Mountain Tuff,
593 *J. Geophys. Res.*, 104(B11), 25,415–25,425.
- 594 Yamamoto, Y., H. Tsunakawa, and H. Shibuya (2003), Palaeointensity study of the Hawai-
595 ian 1960 lava: implications for possible causes of erroneously high intensities, *Geophys-*
596 *ical Journal International*, 153(1), 263–276.
- 597 Zapletal, K. (1992), Self-reversal of isothermal remanent magnetization in a pyrrhotite
598 (fe_7s_8) crystal, *Physics of the Earth and Planetary Interiors*, 70(3–4), 302–311, doi:
599 10.1016/0031-9201(92)90196-3.

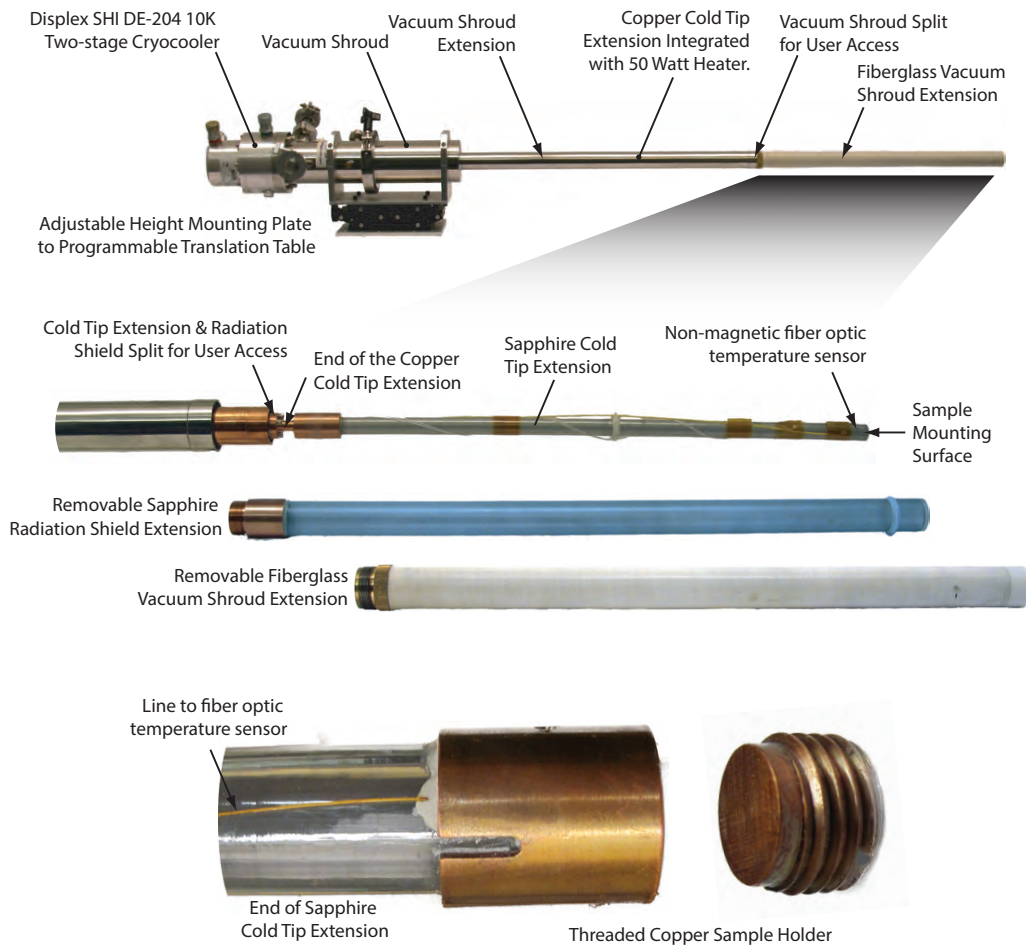


Figure 1. Components of the Institute for Rock Magnetism's low temperature instrument (IRM-LTI). The length of the instrument is 175 cm from the back of the cryocooler to the tip of the fiberglass vacuum shroud.

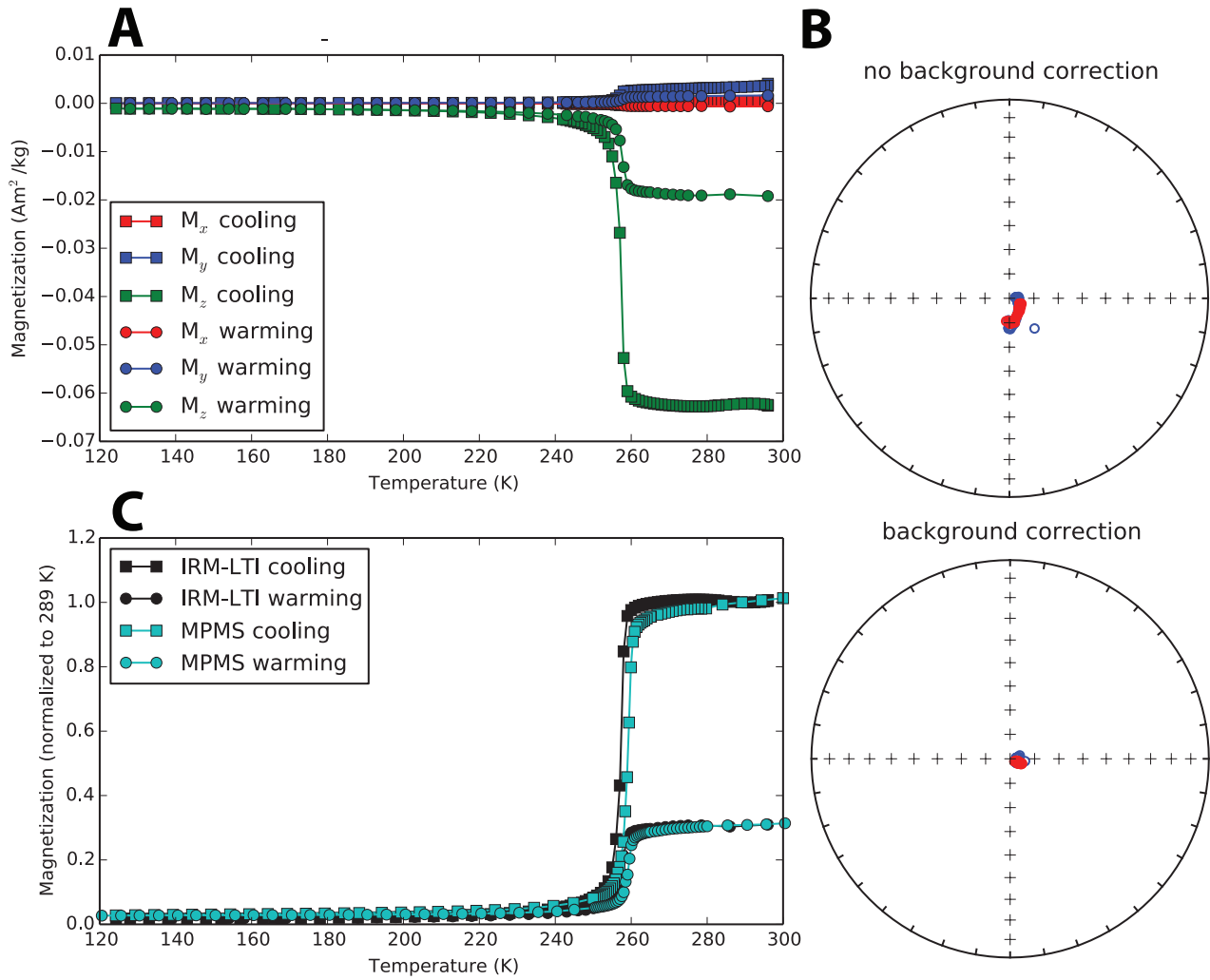


Figure 2. Low temperature thermal cycling of IRMs for a sample of polycrystalline Labrador hematite. (a) Background-corrected three-axis remanence data for a 1.2 T IRM cycled to and from 120 K using the IRM-LTI. There is prominent remanence loss as the specimen cooled through the Morin transition (~ 258 K). (b) Equal area plots of the uncorrected and corrected directions throughout thermal cycling. Blue points are during cooling while red points are during warming. All data plot in the upper hemisphere. (c) Comparison between the total vector magnetization calculated from the three-axis IRM-LTI and 1-axis data collected for a similar experiment conducted on an MPMS.

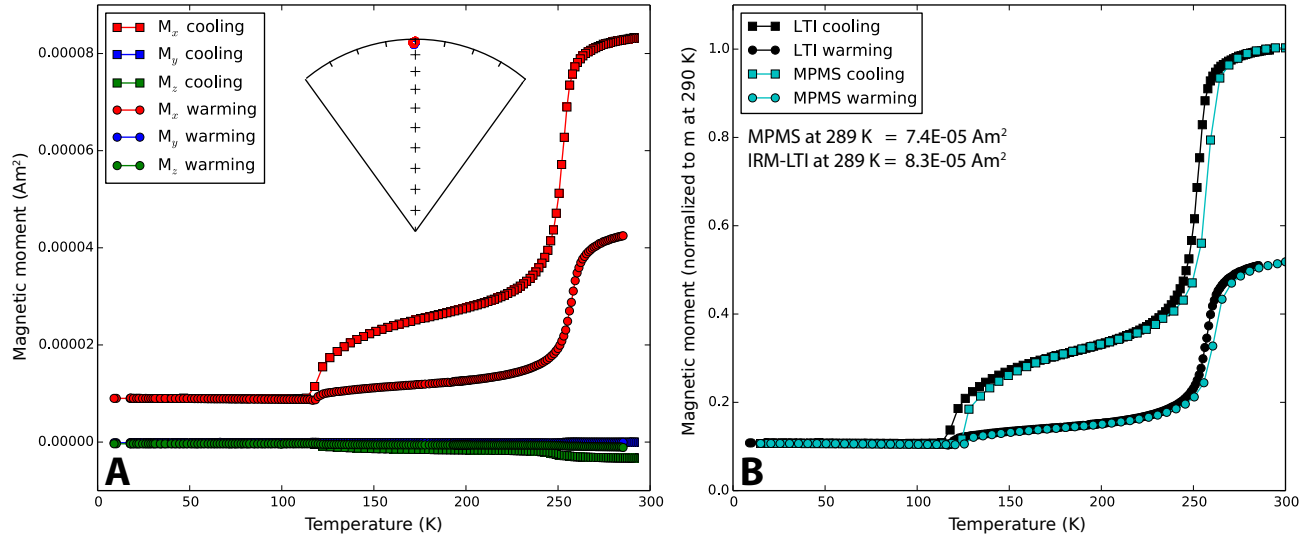


Figure 3. Low temperature thermal cycling of a polycrystalline hematite sample containing trace quantities of magnetite. (a) plot of background-corrected, three-axis remanence data for cooling to 20 K and warming back to room temperature using the IRM-LTI following application of a 1.2 T isothermal remanence. Both the Morin and Verwey transitions are clearly resolved. The inset shows a portion of an equal area plot with the tightly grouped directions of all 114 data points measured during the thermal cycling. (b) plot of the total magnetization measured by the IRM-LTI and single-axis data obtained on an MPMS for a 1.2 T isothermal remanence as it was cycled to and from low temperature (~ 20 K). The data are normalized to the magnetization measured at ~ 290 K on each respective instrument.

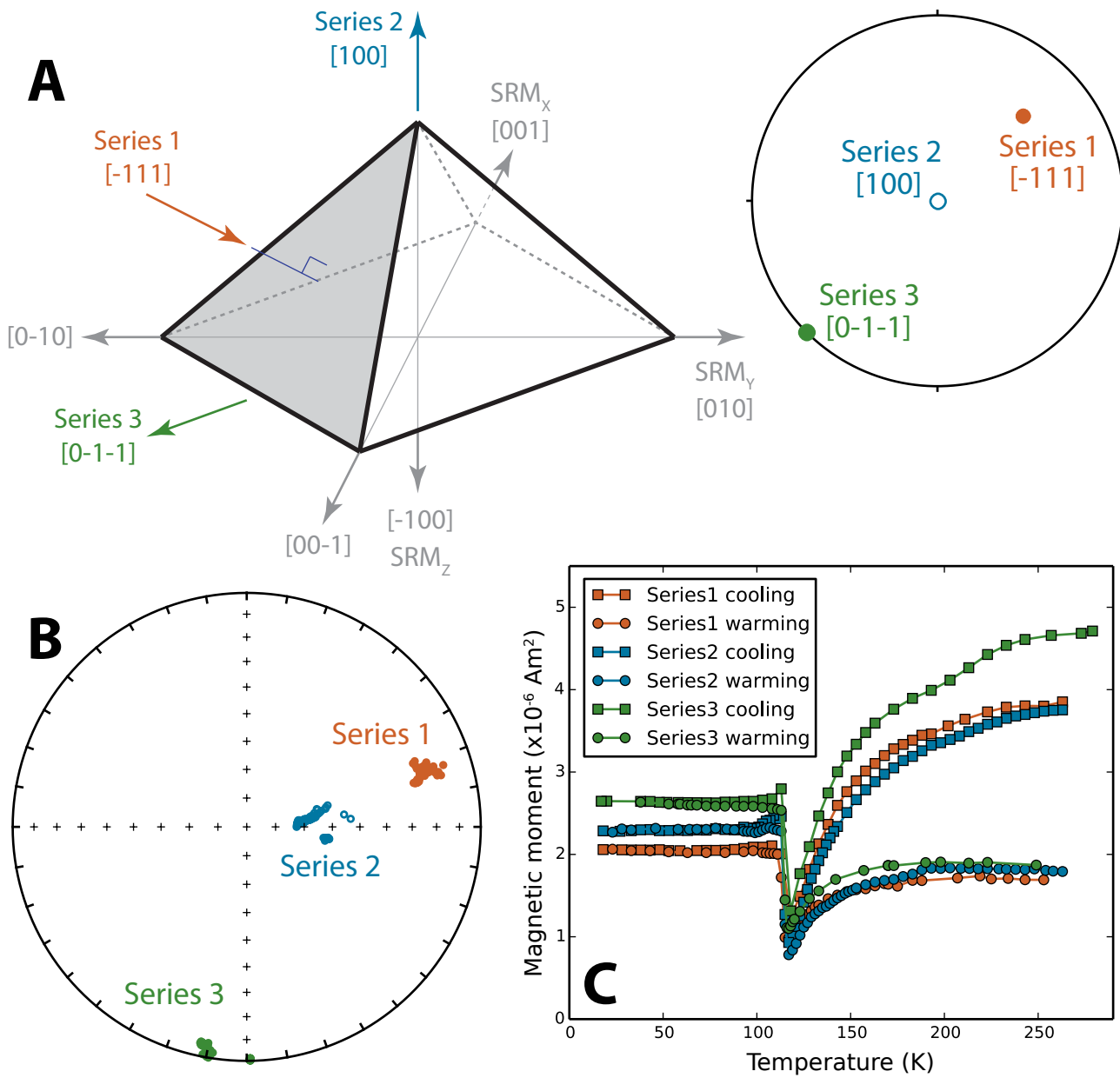


Figure 4. Low temperature thermal cycling of a specimen comprised of a single magnetite crystal. (a) schematic of the specimen depicting the orientation of the crystal axes along with the directions of the isothermal pulse magnetizations applied during the three experiments. (b) equal area plot of the directional data from each experiment. (c) full vector magnetization intensity for each of the three experiments during cooling (squares) and warming (circles).

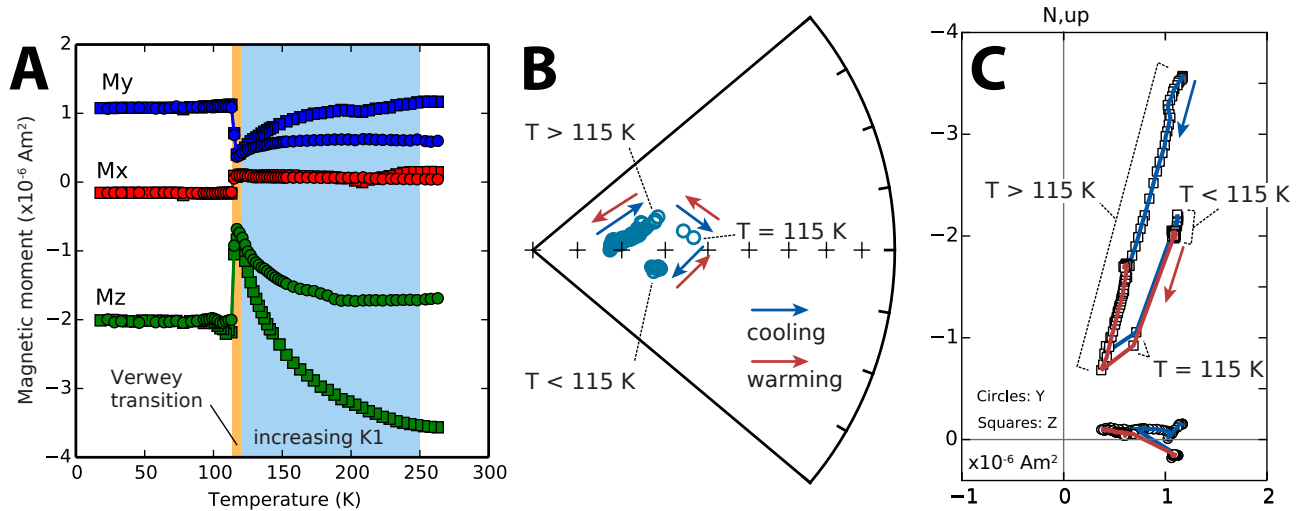


Figure 5. Data from the series 2 experiment (1.2 T IRM applied approximately along the [100] axis) on the single magnetite crystal. (a) three-axis remanence data for cooling to 20 K and warming back to room temperature using the IRM-LTI. The orange box indicates the interval over which the specimen passes through its Verwey transition, while the blue box indicates the interval of remanence loss as the specimen approaches its isotropic point. (b) portion of an equal area plot of the remanence direction during thermal cycling illustrating the clockwise change that occurs as the sample is cooled through the Verwey transition. This directional change is reversible on warming. (c) vector component diagram where both the change in direction and increase in intensity can be seen across the Verwey transition. The blue line connects data points measured during the cooling portion of the experiment while the red line connects data points for the warming portion of the experiment.

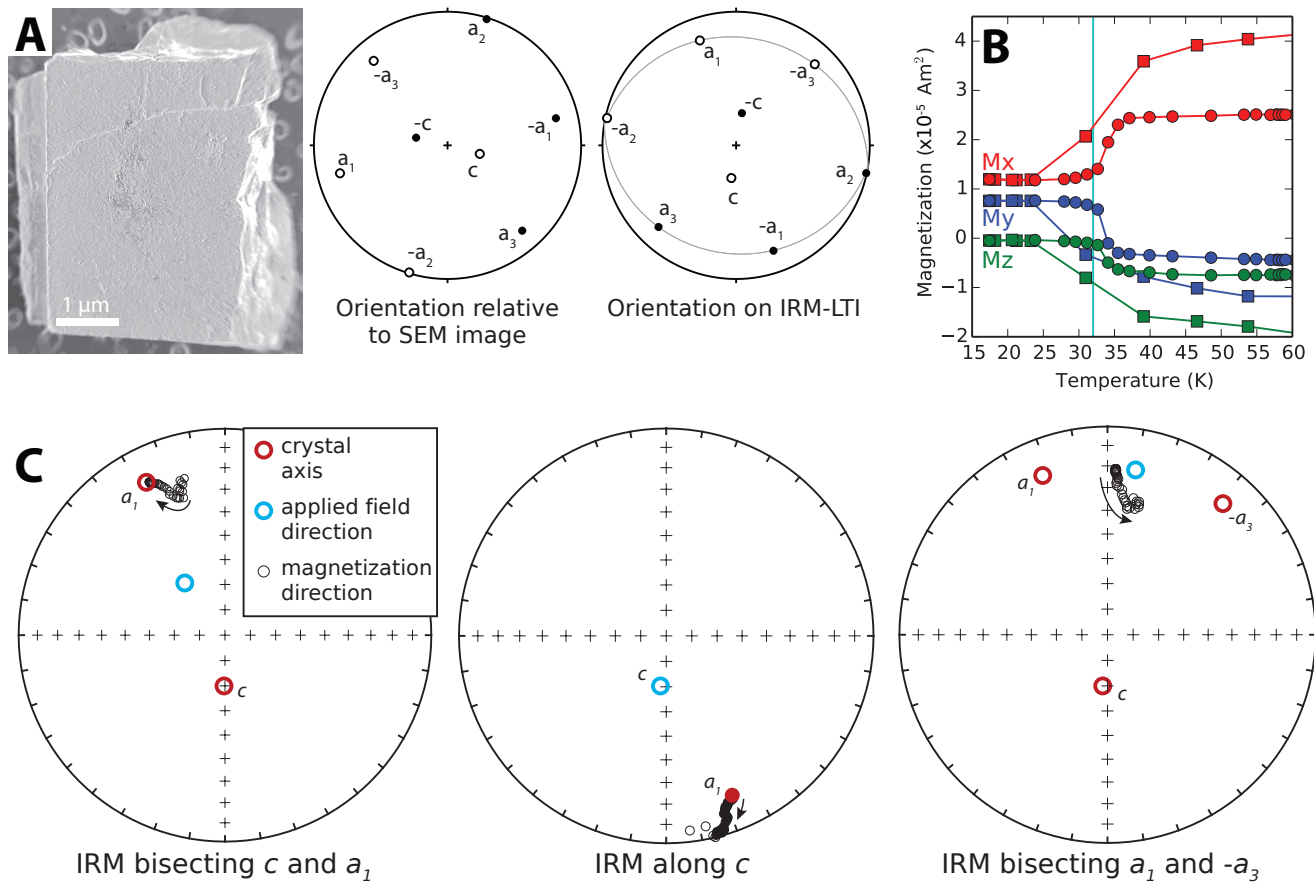


Figure 6. Experiments conducted on a single crystal of pyrrhotite. (a) Secondary electron SEM micrograph of the sample and crystal orientation information during the progression of an experiment. (b) three-axis low-temperature remanence data upon cooling (squares) and warming (circles) for the IRM bisecting c and a_1 experiment. The Besnus transition is well-expressed in these data and closely corresponds with the canonical value for the transition (32 K) shown with the cyan vertical line. (c) Equal area plots showing the directional data (grey circles with arrow indicating direction of change) obtained upon cooling for isothermal remanent magnetizations (IRM) that were applied in three different directions. The direction along which the 1.2 T pulse magnetizations were applied are indicated in each plot with a light blue circle, while relevant crystal axis directions are shown with red circles. *Closed/open circles refer to directions in the lower/upper hemisphere.*

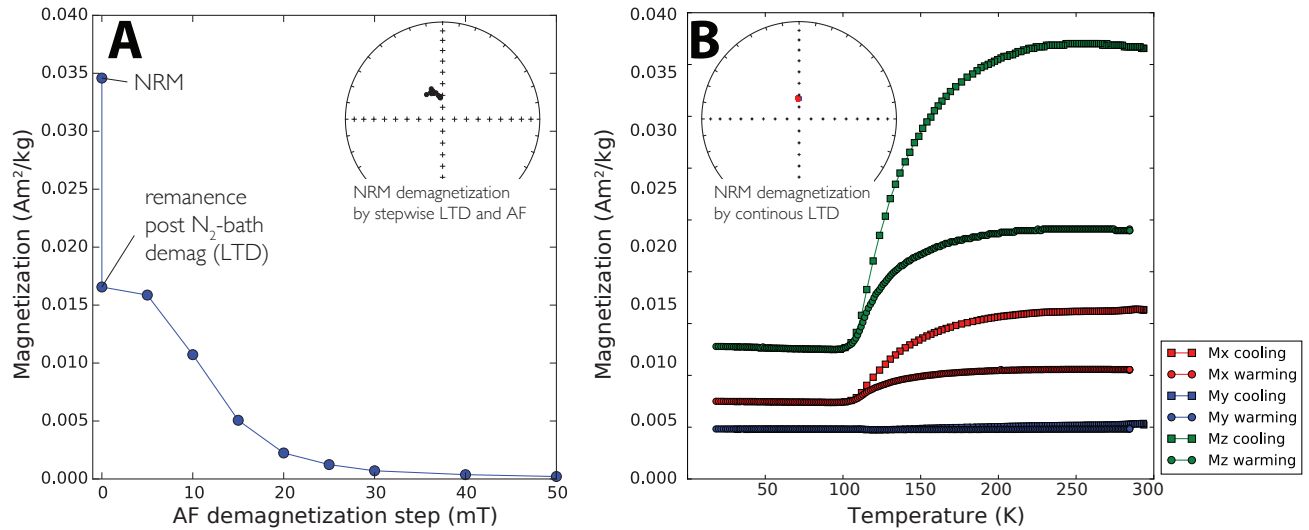


Figure 7. Natural remanent magnetization (NRM) data for a coarse-grained diabase sill sample (PW15-4a). (a) Demagnetization data that begins with a low-temperature demagnetization step (a liquid N_2 bath in near zero field) followed by AF demagnetization. The remanence is comprised of a single directional component as can be seen in the inset equal area plot. (b) Three-axis low-temperature cycling data of NRM obtained on the IRM-LTI for the natural remanence of a sister specimen from the same sample. The directions are summarized on the inset equal area plot and are very similar to the directions of the step-wise AF demagnetization data.

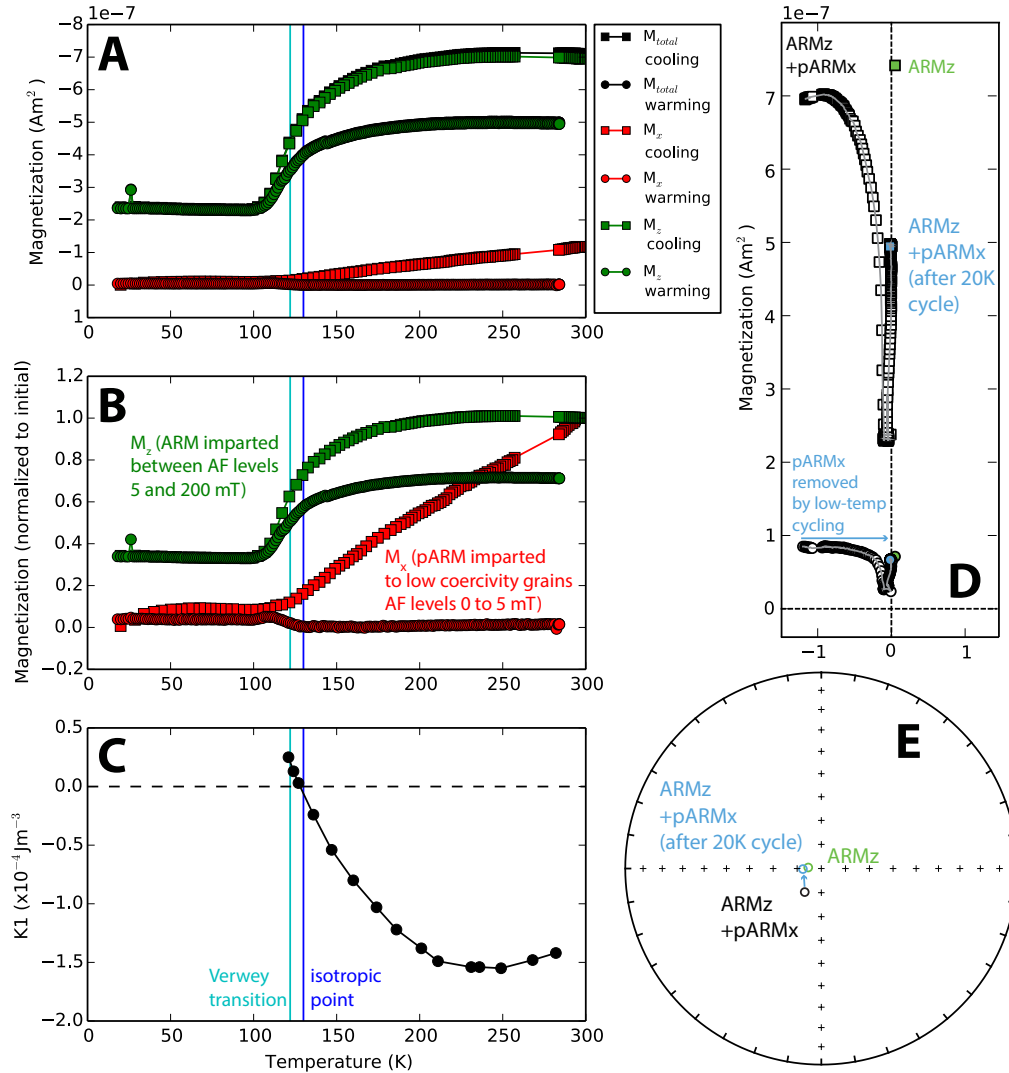


Figure 8. Low-temperature behavior of an ARM applied to the z-axis and a pARM applied to the x-axis of a specimen of an Umkondo diabase sill (PW15-4d). (a) shows the magnetization of the z and x components as well as the total magnetization upon cooling (note that the y-axis of the plot is inverted for comparison between the components and the total magnetization). The z and x components are normalized to their initial magnetizations in (b) to highlight the differing behavior between the x-axis magnetization (pARM imparted to low coercivity grains) and the z-axis magnetization (ARM on the rest of the coercivity spectrum). (c) shows the magnetocrystalline anisotropy constant K_1 as a function of temperature (data of *Bickford et al.* [1957] as presented in *Muxworthy and McClelland* [2000]). The vector-component diagram (d) and equal area plot (e) show the directional change associated with low-temperature cycling and illustrate the return to the direction of the z-axis ARM with the x-axis pARM demagnetized.

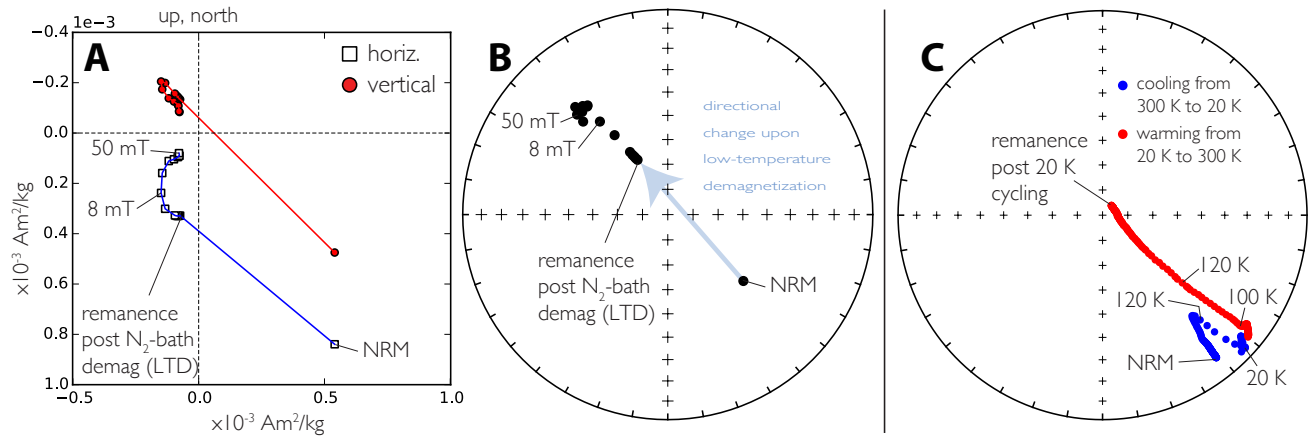


Figure 9. Natural remanent magnetization (NRM) data for a coarse-grained diabase sill sample (PW10-7). (a) Demagnetization data that begins with a low-temperature demagnetization step (a liquid N_2 bath) followed by AF demagnetization. The vector component diagram in (a) and equal area plot in (b) show significant loss of remanence and directional change that accompanied the liquid N_2 treatment. (c) Low-temperature cycling of the NRM of a sister specimen on the IRM-LTI documented directional change throughout the experiment with movement in the direction of overprint removal both during cooling to the Verwey transition and upon warming back across the Verwey transition.